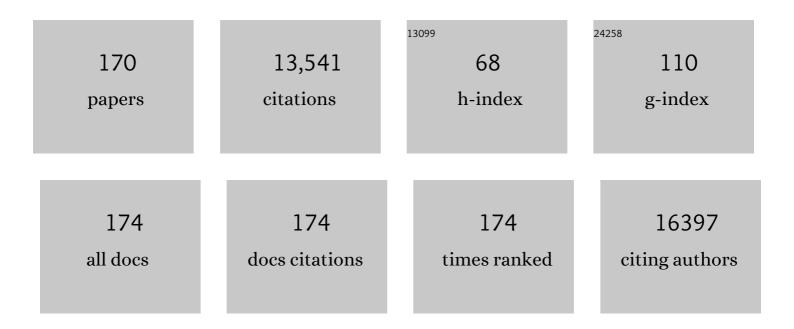
List of Publications by Year in descending order

Source: https://exaly.com/author-pdf/4957443/publications.pdf Version: 2024-02-01



MOO HWAN CHO

#	Article	IF	CITATIONS
1	Semi-Polycrystalline–Polyaniline Empowered Electrochemical Capacitor. Energies, 2022, 15, 2001.	3.1	10
2	Synergistic performance of <scp> Fe <sub>3</sub> O <sub>4</sub> </scp> / <scp> SnO <sub>2</sub> </scp> / <scp>rGO</scp> nanocomposite for supercapacitor and visible lightâ€responsive photocatalysis. International Journal of Energy Research, 2022, 46, 6517-6528.	4.5	10
3	Green and Phytogenic Fabrication of Co-Doped SnO2 Using Aqueous Leaf Extract of Tradescantia spathacea for Photoantioxidant and Photocatalytic Studies. BioNanoScience, 2021, 11, 120-135.	3.5	12
4	Fabrication of binary SnO2/TiO2 nanocomposites under a sonication-assisted approach: Tuning of band-gap and water depollution applications under visible light irradiation. Ceramics International, 2021, 47, 15073-15081.	4.8	36
5	Graphitic‑carbon nitride based mixed-phase bismuth nanostructures: Tuned optical and structural properties with boosted photocatalytic performance for wastewater decontamination under visible-light irradiation. NanoImpact, 2021, 23, 100345.	4.5	8
6	Ag-modified SnO2-graphitic-carbon nitride nanostructures for electrochemical sensor applications. Ceramics International, 2021, 47, 23578-23589.	4.8	36
7	Adsorption promoted visible-light-induced photocatalytic degradation of antibiotic tetracycline by tin oxide/cerium oxide nanocomposite. Applied Surface Science, 2021, 565, 150337.	6.1	62
8	A sensitive electrochemical detection of hydrazine based on SnO2/CeO2 nanostructured oxide. Microchemical Journal, 2021, 171, 106784.	4.5	38
9	Aerogel and its composites for sensing, adsorption, and photocatalysis. , 2021, , 125-144.		1
10	Sulfur-doped-graphitic-carbon nitride (S-g-C3N4) for low cost electrochemical sensing of hydrazine. Journal of Alloys and Compounds, 2020, 816, 152522.	5.5	70
11	Effect of nitrogen doping on the catalytic activity of carbon nano-onions for the oxygen reduction reaction in microbial fuel cells. Journal of Industrial and Engineering Chemistry, 2020, 81, 269-277.	5.8	34
12	Nanoparticles based Surface Plasmon Enhanced Photocatalysis. Environmental Chemistry for A Sustainable World, 2020, , 133-143.	0.5	6
13	Effect of Co2+ and Ni2+ co-doping on SnO2 synthesized via phytogenic method for photoantioxidant studies and photoconversion of 4-nitrophenol. Materials Today Communications, 2020, 25, 101677.	1.9	15
14	Photoantioxidant studies of SnO2 nanoparticles fabricated using aqueous leaf extract of Tradescantia spathacea. Solid State Sciences, 2020, 105, 106279.	3.2	33
15	Effect of Ni-doping on properties of the SnO2 synthesized using Tradescantia spathacea for photoantioxidant studies. Materials Chemistry and Physics, 2020, 252, 123293.	4.0	32
16	Bio-sorbents, industrially important chemicals and novel materials from citrus processing waste as a sustainable and renewable bioresource: A review. Journal of Advanced Research, 2020, 23, 61-82.	9.5	94
17	Microbial fuel cell-assisted biogenic synthesis of gold nanoparticles and its application to energy production and hydrogen peroxide detection. Korean Journal of Chemical Engineering, 2020, 37, 1241-1250.	2.7	16
18	Na,O-co-doped-graphitic-carbon nitride (Na,O-g-C3N4) for nonenzymatic electrochemical sensing of hydrogen peroxide. Applied Surface Science, 2020, 525, 146353.	6.1	45

#	Article	IF	CITATIONS
19	Biofilm-Assisted Fabrication of Ag@SnO <sub>2</sub> - <i>g</i> -C <sub>3</sub> N <sub>4</sub> Nanostructures for Visible Light-Induced Photocatalysis and Photoelectrochemical Performance. Journal of Physical Chemistry C, 2019, 123, 20936-20948.	3.1	60
20	Carbothermal process-derived porous N-doped carbon for flexible energy storage: Influence of carbon surface area and conductivity. Chemical Engineering Journal, 2019, 378, 122158.	12.7	19
21	Synergistically effective and highly visible light responsive SnO2-g-C3N4 nanostructures for improved photocatalytic and photoelectrochemical performance. Applied Surface Science, 2019, 495, 143432.	6.1	77
22	Modern Extraction and Purification Techniques for Obtaining High Purity Food-Grade Bioactive Compounds and Value-Added Co-Products from Citrus Wastes. Foods, 2019, 8, 523.	4.3	155
23	Conducting Polymer Nanocomposites as Gas Sensors. Polymers and Polymeric Composites, 2019, , 911-940.	0.6	3
24	Surface Plasmon-Based Nanomaterials as Photocatalyst. Environmental Chemistry for A Sustainable World, 2019, , 173-187.	0.5	6
25	Phytogenic Synthesis of Band Gap-Narrowed ZnO Nanoparticles Using the Bulb Extract of Costus woodsonii. BioNanoScience, 2019, 9, 334-344.	3.5	37
26	Bio-synthesis of finely distributed Ag nanoparticle-decorated TiO2 nanorods for sunlight-induced photoelectrochemical water splitting. Journal of Industrial and Engineering Chemistry, 2019, 69, 48-56.	5.8	14
27	Conducting Polymer Nanocomposites as Gas Sensors. Polymers and Polymeric Composites, 2019, , 1-30.	0.6	1
28	Feasibility of using hollow double walled Mn2O3 nanocubes for hybrid Na-air battery. Chemical Engineering Journal, 2019, 360, 415-422.	12.7	31
29	Potentials of Costus woodsonii leaf extract in producing narrow band gap ZnO nanoparticles. Materials Science in Semiconductor Processing, 2019, 91, 194-200.	4.0	84
30	Recent progress of algae and blue–green algae-assisted synthesis of gold nanoparticles for various applications. Bioprocess and Biosystems Engineering, 2019, 42, 1-15.	3.4	76
31	Citrus essential oils: Extraction, authentication and application in food preservation. Critical Reviews in Food Science and Nutrition, 2019, 59, 611-625.	10.3	148
32	Simple and sustainable route for large scale fabrication of few layered molybdenum disulfide sheets towards superior adsorption of the hazardous organic pollutant. Journal of Materials Science: Materials in Electronics, 2018, 29, 7792-7800.	2.2	13
33	Lithium ion storage ability, supercapacitor electrode performance, and photocatalytic performance of tungsten disulfide nanosheets. New Journal of Chemistry, 2018, 42, 5859-5867.	2.8	39
34	Ternary Composite of Polyaniline Graphene and TiO <sub>2</sub> as a Bifunctional Catalyst to Enhance the Performance of Both the Bioanode and Cathode of a Microbial Fuel Cell. Industrial & Engineering Chemistry Research, 2018, 57, 6705-6713.	3.7	40
35	Pilot-scale produced super activated carbon with a nanoporous texture as an excellent adsorbent for the efficient removal of metanil yellow. Powder Technology, 2018, 333, 243-251.	4.2	9
36	Environmentally sustainable biogenic fabrication of AuNP decorated-graphitic g-C <sub>3</sub> N <sub>4</sub> nanostructures towards improved photoelectrochemical performances. RSC Advances, 2018, 8, 13898-13909.	3.6	50

#	Article	IF	CITATIONS
37	Solid-state symmetrical supercapacitor based on hierarchical flower-like nickel sulfide with shape-controlled morphological evolution. Electrochimica Acta, 2018, 268, 82-93.	5.2	59
38	Microbial fuel cell assisted band gap narrowed TiO2 for visible light-induced photocatalytic activities and power generation. Scientific Reports, 2018, 8, 1723.	3.3	91
39	Facile Synthesis of SnS <sub>2</sub> Nanostructures with Different Morphologies for High-Performance Supercapacitor Applications. ACS Omega, 2018, 3, 1581-1588.	3.5	125
40	Positively Charged Gold Nanoparticles for Hydrogen Peroxide Detection. BioNanoScience, 2018, 8, 537-543.	3.5	11
41	Citrus waste derived nutra-/pharmaceuticals for health benefits: Current trends and future perspectives. Journal of Functional Foods, 2018, 40, 307-316.	3.4	189
42	Electrochemically active biofilm-assisted biogenic synthesis of an Ag-decorated ZnO@C core–shell ternary plasmonic photocatalyst with enhanced visible-photocatalytic activity. New Journal of Chemistry, 2018, 42, 1995-2005.	2.8	27
43	Recent progress of metal–graphene nanostructures in photocatalysis. Nanoscale, 2018, 10, 9427-9440.	5.6	89
44	Fungi-assisted silver nanoparticle synthesis and their applications. Bioprocess and Biosystems Engineering, 2018, 41, 1-20.	3.4	151
45	A metal-free and non-precious multifunctional 3D carbon foam for high-energy density supercapacitors and enhanced power generation in microbial fuel cells. Journal of Industrial and Engineering Chemistry, 2018, 60, 431-440.	5.8	27
46	Development of Suitable Anode Materials for Microbial Fuel Cells. , 2018, , 101-124.		3
47	A polyaniline@MoS <sub>2</sub> -based organic–inorganic nanohybrid for the removal of Congo red: adsorption kinetic, thermodynamic and isotherm studies. New Journal of Chemistry, 2018, 42, 18802-18809.	2.8	42
48	Environmentally Sustainable Fabrication of Ag@ <i>g-</i> C <sub>3</sub> N <sub>4</sub> Nanostructures and Their Multifunctional Efficacy as Antibacterial Agents and Photocatalysts. ACS Applied Nano Materials, 2018, 1, 2912-2922.	5.0	142
49	Effect of Gallium doping on CdS thin film properties and corresponding Cu(InGa)Se2/CdS:Ga solar cell performance. Thin Solid Films, 2018, 660, 207-212.	1.8	21
50	Defected graphene nano-platelets for enhanced hydrophilic nature and visible light-induced photoelectrochemical performances. Journal of Physics and Chemistry of Solids, 2017, 104, 233-242.	4.0	27
51	Anion selective pTSA doped polyaniline@graphene oxide-multiwalled carbon nanotube composite for Cr(VI) and Congo red adsorption. Journal of Colloid and Interface Science, 2017, 496, 407-415.	9.4	159
52	Simple and Large Scale Construction of MoS2-g-C3N4 Heterostructures Using Mechanochemistry for High Performance Electrochemical Supercapacitor and Visible Light Photocatalytic Applications. Scientific Reports, 2017, 7, 43055.	3.3	157
53	Growth of three-dimensional flower-like SnS <sub>2</sub> on g-C <sub>3</sub> N <sub>4</sub> sheets as an efficient visible-light photocatalyst, photoelectrode, and electrochemical supercapacitance material. Sustainable Energy and Fuels, 2017, 1, 510-519.	4.9	59
54	Mechanically exfoliated MoS2 sheet coupled with conductive polyaniline as a superior supercapacitor electrode material. Journal of Colloid and Interface Science, 2017, 504, 276-282.	9.4	91

#	Article	IF	CITATIONS
55	Three-dimensional SnS2 nanopetals for hybrid sodium-air batteries. Electrochimica Acta, 2017, 257, 328-334.	5.2	53
56	Binder-free production of 3D N-doped porous carbon cubes for efficient Pb2+ removal through batch and fixed bed adsorption. Journal of Cleaner Production, 2017, 168, 290-301.	9.3	29
57	Facile and sustainable synthesis of carbon-doped ZnO nanostructures towards the superior visible light photocatalytic performance. New Journal of Chemistry, 2017, 41, 9314-9320.	2.8	102
58	Manganese dioxide nanorods intercalated reduced graphene oxide nanocomposite toward high performance electrochemical supercapacitive electrode materials. Journal of Colloid and Interface Science, 2017, 506, 613-619.	9.4	34
59	Ce3+-ion, Surface Oxygen Vacancy, and Visible Light-induced Photocatalytic Dye Degradation and Photocapacitive Performance of CeO2-Graphene Nanostructures. Scientific Reports, 2017, 7, 5928.	3.3	133
60	Intercalated reduced graphene oxide and its content effect on the supercapacitance performance of the three dimensional flower-like β-Ni(OH) <sub>2</sub> architecture. New Journal of Chemistry, 2017, 41, 10467-10475.	2.8	20
61	Effect of polyaniline concentration on the photoconversion efficiency of nano-TiO2 based dye sensitized solar cells. Journal of Materials Science: Materials in Electronics, 2017, 28, 3210-3216.	2.2	2
62	Simple and rapid synthesis of ternary polyaniline/titanium oxide/graphene by simultaneous TiO2 generation and aniline oxidation as hybrid materials for supercapacitor applications. Journal of Solid State Electrochemistry, 2017, 21, 57-68.	2.5	56
63	Converting citrus wastes into value-added products: Economic and environmently friendly approaches. Nutrition, 2017, 34, 29-46.	2.4	356
64	Metal-Free Carbon-Based Materials: Promising Electrocatalysts for Oxygen Reduction Reaction in Microbial Fuel Cells. International Journal of Molecular Sciences, 2017, 18, 25.	4.1	67
65	Self-Assembled 3D Flower-Like Nickel Hydroxide Nanostructures and Their Supercapacitor Applications. Scientific Reports, 2016, 6, 27318.	3.3	127
66	Earth-abundant stable elemental semiconductor red phosphorus-based hybrids for environmental remediation and energy storage applications. RSC Advances, 2016, 6, 44616-44629.	3.6	56
67	Graphene integrated polyaniline nanostructured composite coating for protecting steels from corrosion: Synthesis, characterization, and protection mechanism of the coating material in acidic environment. Construction and Building Materials, 2016, 115, 618-633.	7.2	44
68	CdS-graphene Nanocomposite for Efficient Visible-light-driven Photocatalytic and Photoelectrochemical Applications. Journal of Colloid and Interface Science, 2016, 482, 221-232.	9.4	140
69	Facile and single-step route towards ZnO@C core–shell nanoparticles as an oxygen vacancy induced visible light active photocatalyst using the thermal decomposition of Zn(an)2(NO3)2. RSC Advances, 2016, 6, 70644-70652.	3.6	13
70	Facile and Scale Up Synthesis of Red Phosphorus-Graphitic Carbon Nitride Heterostructures for Energy and Environment Applications. Scientific Reports, 2016, 6, 27713.	3.3	56
71	Facile route to a conducting ternary polyaniline@TiO <sub>2</sub> /GN nanocomposite for environmentally benign applications: photocatalytic degradation of pollutants and biological activity. RSC Advances, 2016, 6, 111308-111317.	3.6	45
72	Electrochemically synthesized sulfur-doped graphene as a superior metal-free cathodic catalyst for oxygen reduction reaction in microbial fuel cells. RSC Advances, 2016, 6, 103446-103454.	3.6	31

#	Article	IF	CITATIONS
73	Highly Visible Light Responsive, Narrow Band gap TiO2 Nanoparticles Modified by Elemental Red Phosphorus for Photocatalysis and Photoelectrochemical Applications. Scientific Reports, 2016, 6, 25405.	3.3	222
74	Enhanced electrochemical behavior and hydrophobicity of crystalline polyaniline@graphene nanocomposite synthesized at elevated temperature. Composites Part B: Engineering, 2016, 87, 281-290.	12.0	94
75	Metal free earth abundant elemental red phosphorus: a new class of visible light photocatalyst and photoelectrode materials. Physical Chemistry Chemical Physics, 2016, 18, 3921-3928.	2.8	74
76	Simultaneous sulfur doping and exfoliation of graphene from graphite using an electrochemical method for supercapacitor electrode materials. Journal of Materials Chemistry A, 2016, 4, 233-240.	10.3	151
77	Nitrogen-doped titanium dioxide (N-doped TiO <sub>2</sub> ) for visible light photocatalysis. New Journal of Chemistry, 2016, 40, 3000-3009.	2.8	549
78	Fabrication of WO <sub>3</sub> nanorods on graphene nanosheets for improved visible light-induced photocapacitive and photocatalytic performance. RSC Advances, 2016, 6, 20824-20833.	3.6	121
79	Three-dimensional, highly porous N-doped carbon foam as microorganism propitious, efficient anode for high performance microbial fuel cell. RSC Advances, 2016, 6, 25799-25807.	3.6	44
80	Fibrous polyaniline@manganese oxide nanocomposites as supercapacitor electrode materials and cathode catalysts for improved power production in microbial fuel cells. Physical Chemistry Chemical Physics, 2016, 18, 9053-9060.	2.8	133
81	Route to High Surface Area, Mesoporosity of Polyaniline–Titanium Dioxide Nanocomposites via One Pot Synthesis for Energy Storage Applications. Industrial & Engineering Chemistry Research, 2016, 55, 116-124.	3.7	70
82	Anchoring Mechanism of ZnO Nanoparticles on Graphitic Carbon Nanofiber Surfaces through a Modified Coâ€Precipitation Method to Improve Interfacial Contact and Photocatalytic Performance. ChemPhysChem, 2015, 16, 3214-3232.	2.1	37
83	Silver nanoparticles and defect-induced visible light photocatalytic and photoelectrochemical performance of Ag@m-TiO2 nanocomposite. Solar Energy Materials and Solar Cells, 2015, 141, 162-170.	6.2	126
84	Improved electrode performance in microbial fuel cells and the enhanced visible light-induced photoelectrochemical behaviour of PtO @M-TiO2 nanocomposites. Ceramics International, 2015, 41, 9131-9139.	4.8	39
85	Red wines and flavonoids diminish <i>Staphylococcus aureus</i> virulence with anti-biofilm and anti-hemolytic activities. Biofouling, 2015, 31, 1-11.	2.2	94
86	Electrical conductivity, optical property and ammonia sensing studies on HCl Doped Au@polyaniline nanocomposites. Electronic Materials Letters, 2015, 11, 1-6.	2.2	28
87	Visible light-induced enhanced photoelectrochemical and photocatalytic studies of gold decorated SnO <sub>2</sub> nanostructures. New Journal of Chemistry, 2015, 39, 2758-2766.	2.8	101
88	Green synthesis, photocatalytic and photoelectrochemical performance of an Au–Graphene nanocomposite. RSC Advances, 2015, 5, 26897-26904.	3.6	80
89	Polythiophene nanocomposites for photodegradation applications: Past, present and future. Journal of Saudi Chemical Society, 2015, 19, 494-504.	5.2	91
90	DC electrical conductivity retention and electrical compensation of polyaniline by TiO2 at higher loading percentages in polyaniline@TiO2 nanocomposites. Electronic Materials Letters, 2015, 11, 559-564.	2.2	11

#	Article	IF	CITATIONS
91	Eco-friendly, catalyst-free synthesis of highly pure carbon spheres using vegetable oils as a renewable source and their application as a template for ZnO and MgO hollow spheres. RSC Advances, 2015, 5, 57114-57121.	3.6	5
92	Facile strategy for the synthesis of non-covalently bonded and para-toluene sulfonic acid-functionalized fibrous polyaniline@graphene–PVC nanocomposite for the removal of Congo red. New Journal of Chemistry, 2015, 39, 7004-7011.	2.8	21
93	Simple route for the generation of differently functionalized PVC@graphene–polyaniline fiber bundles for the removal of Congo red from wastewater. RSC Advances, 2015, 5, 61486-61494.	3.6	38
94	Simple route for gram synthesis of less defective few layered graphene and its electrochemical performance. RSC Advances, 2015, 5, 44920-44927.	3.6	38
95	A low temperature bottom-up approach for the synthesis of few layered graphene nanosheets via C–C bond formation using a modified Ullmann reaction. RSC Advances, 2015, 5, 46589-46597.	3.6	33
96	The multifaceted roles of the interspecies signalling molecule indole in <scp><i>A</i></scp> <i>grobacterium tumefaciens</i> . Environmental Microbiology, 2015, 17, 1234-1244.	3.8	54
97	Gold nanoparticles-sensitized wide and narrow band gap TiO <sub>2</sub> for visible light applications: a comparative study. New Journal of Chemistry, 2015, 39, 4708-4715.	2.8	90
98	Facile electrochemical assisted synthesis of ZnO/graphene nanosheets with enhanced photocatalytic activity. RSC Advances, 2015, 5, 97788-97797.	3.6	39
99	Graphene nanodiscs from electrochemical assisted micromechanical exfoliation of graphite: Morphology and supramolecular behavior. Materials Express, 2015, 5, 471-479.	0.5	15
100	Synthesis of highly crystalline polyaniline nanoparticles by simple chemical route. Materials Letters, 2015, 161, 372-374.	2.6	21
101	Biogenic synthesis of a Ag–graphene nanocomposite with efficient photocatalytic degradation, electrical conductivity and photoelectrochemical performance. New Journal of Chemistry, 2015, 39, 8121-8129.	2.8	130
102	Electrically conductive polyaniline sensitized defective-TiO <sub>2</sub> for improved visible light photocatalytic and photoelectrochemical performance: a synergistic effect. New Journal of Chemistry, 2015, 39, 8381-8388.	2.8	42
103	Ammonia sensing and DC electrical conductivity studies of p-toluene sulfonic acid doped cetyltrimethylammonium bromide assisted V2O5@polyaniline composite nanofibers. Journal of Industrial and Engineering Chemistry, 2015, 22, 147-152.	5.8	23
104	Au@TiO2 nanocomposites for the catalytic degradation of methyl orange and methylene blue: An electron relay effect. Journal of Industrial and Engineering Chemistry, 2014, 20, 1584-1590.	5.8	234
105	Highly visible light active Ag@ZnO nanocomposites synthesized by gel-combustion route. Journal of Industrial and Engineering Chemistry, 2014, 20, 1602-1607.	5.8	104
106	Cinkgolic acids and Ginkgo biloba extract inhibit Escherichia coli O157:H7 and Staphylococcus aureus biofilm formation. International Journal of Food Microbiology, 2014, 174, 47-55.	4.7	114
107	Band gap engineering of CeO <sub>2</sub> nanostructure using an electrochemically active biofilm for visible light applications. RSC Advances, 2014, 4, 16782-16791.	3.6	266
108	pTSA doped conducting graphene/polyaniline nanocomposite fibers: Thermoelectric behavior and electrode analysis. Chemical Engineering Journal, 2014, 242, 155-161.	12.7	73

#	Article	IF	CITATIONS
109	Band gap engineered TiO <sub>2</sub> nanoparticles for visible light induced photoelectrochemical and photocatalytic studies. Journal of Materials Chemistry A, 2014, 2, 637-644.	10.3	751
110	Ammonia vapor sensing and electrical properties of fibrous multi-walled carbon nanotube/polyaniline nanocomposites prepared in presence of cetyl-trimethylammonium bromide. Journal of Industrial and Engineering Chemistry, 2014, 20, 2010-2017.	5.8	41
111	Enhanced thermoelectric performance and ammonia sensing properties of sulfonated polyaniline/graphene thin films. Materials Letters, 2014, 114, 159-162.	2.6	46
112	Enhanced thermoelectric behaviour and visible light activity of Ag@TiO <sub>2</sub> /polyaniline nanocomposite synthesized by biogenic-chemical route. RSC Advances, 2014, 4, 23713-23719.	3.6	75
113	Thermoresponsive oligomers reduce <i>Escherichia coli</i> O157:H7 biofouling and virulence. Biofouling, 2014, 30, 627-637.	2.2	10
114	Anti-biofilm, anti-hemolysis, and anti-virulence activities of black pepper, cananga, myrrh oils, and nerolidol against Staphylococcus aureus. Applied Microbiology and Biotechnology, 2014, 98, 9447-9457.	3.6	84
115	Electrochemically active biofilm assisted synthesis of Ag@CeO2 nanocomposites for antimicrobial activity, photocatalysis and photoelectrodes. Journal of Colloid and Interface Science, 2014, 431, 255-263.	9.4	102
116	Highly photoactive SnO <sub>2</sub> nanostructures engineered by electrochemically active biofilm. New Journal of Chemistry, 2014, 38, 2462-2469.	2.8	66
117	Stilbenes ReduceStaphylococcus aureusHemolysis, Biofilm Formation, and Virulence. Foodborne Pathogens and Disease, 2014, 11, 710-717.	1.8	60
118	Indole oxidation enhances electricity production in an E. coli-catalyzed microbial fuel cell. Biotechnology and Bioprocess Engineering, 2014, 19, 126-131.	2.6	20
119	Mixed Culture Electrochemically Active Biofilms and their Microscopic and Spectroelectrochemical Studies. ACS Sustainable Chemistry and Engineering, 2014, 2, 423-432.	6.7	46
120	Optimization of positively charged gold nanoparticles synthesized using a stainless-steel mesh and its application for colorimetric hydrogen peroxide detection. Journal of Industrial and Engineering Chemistry, 2014, 20, 2003-2009.	5.8	19
121	Resveratrol Oligomers Inhibit Biofilm Formation of <i>Escherichia coli</i> O157:H7 and <i>Pseudomonas aeruginosa</i> . Journal of Natural Products, 2014, 77, 168-172.	3.0	61
122	Defect-Induced Band Gap Narrowed CeO <sub>2</sub> Nanostructures for Visible Light Activities. Industrial & Engineering Chemistry Research, 2014, 53, 9754-9763.	3.7	278
123	Coumarins reduce biofilm formation and the virulence of Escherichia coli O157:H7. Phytomedicine, 2014, 21, 1037-1042.	5.3	130
124	Biogenic Fabrication of Au@CeO <sub>2</sub> Nanocomposite with Enhanced Visible Light Activity. Journal of Physical Chemistry C, 2014, 118, 9477-9484.	3.1	123
125	Enhanced Thermal Stability under DC Electrical Conductivity Retention and Visible Light Activity of Ag/TiO <sub>2</sub> @Polyaniline Nanocomposite Film. ACS Applied Materials & Interfaces, 2014, 6, 8124-8133.	8.0	81
126	Visible light-driven photocatalytic and photoelectrochemical studies of Ag–SnO <sub>2</sub> nanocomposites synthesized using an electrochemically active biofilm. RSC Advances, 2014, 4, 26013-26021.	3.6	103

#	Article	IF	CITATIONS
127	ZnO nanoparticles inhibit Pseudomonas aeruginosa biofilm formation and virulence factor production. Microbiological Research, 2014, 169, 888-896.	5.3	196
128	Novel Ag@TiO2 nanocomposite synthesized by electrochemically active biofilm for nonenzymatic hydrogen peroxide sensor. Materials Science and Engineering C, 2013, 33, 4692-4699.	7.3	70
129	Oxygen vacancy induced band gap narrowing of ZnO nanostructures by an electrochemically active biofilm. Nanoscale, 2013, 5, 9238.	5.6	523
130	Gold Nanoparticles Produced Inâ€Situ Mediate Bioelectricity and Hydrogen Production in a Microbial Fuel Cell by Quantized Capacitance Charging. ChemSusChem, 2013, 6, 246-250.	6.8	34
131	Indole and 7-benzyloxyindole attenuate the virulence of Staphylococcus aureus. Applied Microbiology and Biotechnology, 2013, 97, 4543-4552.	3.6	98
132	Diverse plant extracts and <i>trans</i> -resveratrol inhibit biofilm formation and swarming of <i>Escherichia coli</i> O157:H7. Biofouling, 2013, 29, 1189-1203.	2.2	78
133	Enhanced optical, visible light catalytic and electrochemical properties of Au@TiO2 nanocomposites. Journal of Industrial and Engineering Chemistry, 2013, 19, 1845-1850.	5.8	29
134	Biogenic Synthesis, Photocatalytic, and Photoelectrochemical Performance of Ag–ZnO Nanocomposite. Journal of Physical Chemistry C, 2013, 117, 27023-27030.	3.1	368
135	Inhibition of Pseudomonas aeruginosa and Escherichia coli O157:H7 Biofilm Formation by Plant Metabolite Îμ-Viniferin. Journal of Agricultural and Food Chemistry, 2013, 61, 7120-7126.	5.2	90
136	Electrochemically active biofilm mediated bio-hydrogen production catalyzed by positively charged gold nanoparticles. International Journal of Hydrogen Energy, 2013, 38, 5243-5250.	7.1	70
137	Catalytic role of Au@TiO2 nanocomposite on enhanced degradation of an azo-dye by electrochemically active biofilms: a quantized charging effect. Journal of Nanoparticle Research, 2013, 15, 1.	1.9	4
138	Highly visible light active Ag@TiO2 nanocomposites synthesized using an electrochemically active biofilm: a novel biogenic approach. Nanoscale, 2013, 5, 4427.	5.6	219
139	Simultaneous Enhancement of Methylene Blue Degradation and Power Generation in a Microbial Fuel Cell by Gold Nanoparticles. Industrial & Engineering Chemistry Research, 2013, 52, 8174-8181.	3.7	81
140	Production of bioelectricity, bio-hydrogen, high value chemicals and bioinspired nanomaterials by electrochemically active biofilms. Biotechnology Advances, 2013, 31, 915-924.	11.7	57
141	Anti-biofilm activities of quercetin and tannic acid against <i>Staphylococcus aureus</i> . Biofouling, 2013, 29, 491-499.	2.2	198
142	Band gap narrowing of titanium dioxide (TiO2) nanocrystals by electrochemically active biofilms and their visible light activity. Nanoscale, 2013, 5, 6323.	5.6	155
143	Synthesis of Positively Charged Gold Nanoparticles Using a Stainless-Steel Mesh. Journal of Nanoscience and Nanotechnology, 2013, 13, 6140-6144.	0.9	15
144	Enhanced Performance of a Microbial Fuel Cell Using CNT/MnO <sub>2</sub> Nanocomposite as a Bioanode Material. Journal of Nanoscience and Nanotechnology, 2013, 13, 7712-7716.	0.9	58

#	Article	IF	CITATIONS
145	Positively Charged Gold Nanoparticles Synthesized by Electrochemically Active Biofilm—A Biogenic Approach. Journal of Nanoscience and Nanotechnology, 2013, 13, 6079-6085.	0.9	44
146	Acceleration of protease effect on Staphylococcus aureus biofilm dispersal. FEMS Microbiology Letters, 2012, 335, 31-38.	1.8	75
147	A simple biogenic route to rapid synthesis of Au@TiO2 nanocomposites by electrochemically active biofilms. Journal of Nanoparticle Research, 2012, 14, 1.	1.9	37
148	Flavone Reduces the Production of Virulence Factors, Staphyloxanthin and α-Hemolysin, in Staphylococcus aureus. Current Microbiology, 2012, 65, 726-732.	2.2	60
149	Efficient decolorization of real dye wastewater and bioelectricity generation using a novel single chamber biocathode-microbial fuel cell. Bioresource Technology, 2012, 119, 22-27.	9.6	76
150	Antibiofilm activity of Streptomyces sp. BFI 230 and Kribbella sp. BFI 1562 against Pseudomonas aeruginosa. Applied Microbiology and Biotechnology, 2012, 96, 1607-1617.	3.6	35
151	Indole-3-acetaldehyde from Rhodococcus sp. BFI 332 inhibits Escherichia coli O157:H7 biofilm formation. Applied Microbiology and Biotechnology, 2012, 96, 1071-1078.	3.6	44
152	7-fluoroindole as an antivirulence compound against Pseudomonas aeruginosa. FEMS Microbiology Letters, 2012, 329, 36-44.	1.8	81
153	Extracellular protease in Actinomycetes culture supernatants inhibits and detaches Staphylococcus aureus biofilm formation. Biotechnology Letters, 2012, 34, 655-661.	2.2	35
154	Electrochemically active biofilm-mediated synthesis of silver nanoparticles in water. Green Chemistry, 2011, 13, 1482.	9.0	78
155	Environmental factors affecting indole production in Escherichia coli. Research in Microbiology, 2011, 162, 108-116.	2.1	102
156	3â€Indolylacetonitrile Decreases <i>Escherichia coli</i> O157:H7 Biofilm Formation and <i>Pseudomonas aeruginosa</i> Virulence. Environmental Microbiology, 2011, 13, 62-73.	3.8	166
157	Granular activated carbon based microbial fuel cell for simultaneous decolorization of real dye wastewater and electricity generation. New Biotechnology, 2011, 29, 32-37.	4.4	102
158	Transcriptomic Analysis for Genetic Mechanisms of the Factors Related to Biofilm Formation in Escherichia coli O157:H7. Current Microbiology, 2011, 62, 1321-1330.	2.2	29
159	Indole and 3-indolylacetonitrile inhibit spore maturation in Paenibacillus alvei. BMC Microbiology, 2011, 11, 119.	3.3	37
160	Apple Flavonoid Phloretin Inhibits Escherichia coli O157:H7 Biofilm Formation and Ameliorates Colon Inflammation in Rats. Infection and Immunity, 2011, 79, 4819-4827.	2.2	180
161	Low concentrations of honey reduce biofilm formation, quorum sensing, and virulence in <i>Escherichia coli</i> O157:H7. Biofouling, 2011, 27, 1095-1104.	2.2	83
162	Antioxidant, antibacterial, tyrosinase inhibitory, and biofilm inhibitory activities of fermented rice bran broth with effective microorganisms. Biotechnology and Bioprocess Engineering, 2010, 15, 139-144.	2.6	11

#	Article	IF	CITATIONS
163	Removal of nitrogen in wastewater by polyvinyl alcohol (PVA)-immobilization of effective microorganisms. Korean Journal of Chemical Engineering, 2010, 27, 193-197.	2.7	30
164	Optimal strategies of fill and aeration in a sequencing batch reactor for biological nitrogen and carbon removal. Korean Journal of Chemical Engineering, 2010, 27, 925-929.	2.7	9
165	Enhanced production of laccase fromTrametes sp. by combination of various inducers. Biotechnology and Bioprocess Engineering, 2006, 11, 96-99.	2.6	18
166	The selective visualization of lignin peroxidase, manganese peroxidase and laccase, produced by white rot fungi on solid media. Biotechnology and Bioprocess Engineering, 2003, 8, 130-134.	2.6	13
167	Characterization of an oxygen-dependent inducible promoter, theEscherichia coli nar promoter, in gram-negative host strains. Biotechnology and Bioengineering, 2003, 82, 271-277.	3.3	4
168	Laccase production from repeated batch cultures using free mycelia of Trametes sp Enzyme and Microbial Technology, 2002, 30, 741-746.	3.2	34
169	Biodegradation of pentachlorophenol by white rot fungi under ligninolytic and nonligninolytic conditions. Biotechnology and Bioprocess Engineering, 2000, 5, 211-214.	2.6	25
170	Enhanced production of cis,cis-muconate in a cell-recycle bioreactor. Journal of Bioscience and Bioengineering, 1997, 84, 70-76.	0.9	28